Increased Rigidity of Domain Structures Enhances the Stability of a Mutant Enzyme Created by Directed Evolution†

Jun Hoseki,‡ Akihiro Okamoto,‡ Naoki Takada,§ Atsushi Suenaga,§ Noriyuki Futatsugi,§ Akihiko Konagaya,§ Makoto Taiji,§ Takato Yano,‡ Seiki Kuramitsu,||,⊥ and Hiroyuki Kagamiyama*,‡

Department of Biochemistry, Osaka Medical College, Takatsuki, Osaka 569-8686, RIKEN Genomic Sciences Center, 1-7-22 Suehiro-cho, Tsurumi, Yokohama 230-0045, Department of Biology, Graduate School of Science, Osaka University, Toyonaka, Osaka 560-0043, and RIKEN Harima Institute at SPring-8, 1-1-1 Kouto, Mikazuki, Sayo-gun, Hyogo 679-5148, Japan

Received May 13, 2003; Revised Manuscript Received August 28, 2003

ABSTRACT: A mutant of kanamycin nucleotidyltransferase (KNT) was previously created by directed evolution. This mutant, HTK, has 19 amino acid substitutions, which increase the thermostability by 20 °C. In this study, we have examined to what extent each mutation contributes to the increased stability and analyzed how the mutations affect the structure of KNT at 72 °C using molecular dynamics simulations. The effects of some mutations on the stability are simply additive, but those of others are cooperative. Mutations with large effects on the stability are introduced into the N-terminal domain, which appears to be less stable than the C-terminal domain. Results of the molecular dynamics simulations have indicated that the rigidity of the domain structures is increased by the mutations: at 72 °C, the intradomain fluctuations of HTK are decreased, and in turn, its interdomain motions are pronounced, whereas the structure of the preevolved KNT fluctuates randomly. Chemical modification experiments of cysteine residues have shown that the cysteine residues of HTK are less accessible to an SH reagent than those of the preevolved KNT. The present results suggest that the 19 mutations of HTK stabilize KNT by affecting the dynamic behavior of the structure of this enzyme without significantly changing its static overall structure.

Although directed evolution has proved to be a powerful method for protein engineering (*1*), few mutants obtained by directed evolution have been analyzed in detail. Analysis of those mutants would, however, provide new insights into the structure−function relationship or structure formation of proteins, especially when mutations are introduced into unexpected sites. For example, the analysis of a mutant asparate aminotransferase, the catalytic efficiency for valine of which is increased 10^6-fold by directed evolution, has revealed how residues remote from the active site affect the substrate specificity of an enzyme through their effects on the domain motion of the enzyme (*2*−*4*). Also, the organophilic mutant of *p*-nitrobenzyl esterase created by directed evolution has amino acid substitutions outside the active site (*5*, *6*). Information from such "retrospective" studies, where mutants with altered properties are created first and analyzed later, should complement that from conventional studies, where rationally designed mutations are introduced and then their effects are analyzed and interpreted in the context of the proposed mechanism.

We have recently increased the thermostability of kanamycin nucleotidyltransferase (KNT)[1] using directed evolution performed in an extremely thermophilic bacterium, *Thurmus thermophilus* (*7*), to create a convenient selection marker for functional genomics studies on this bacterium (*8*). Briefly, directed evolution was started from a mutant of the *Staphylococcus aureus* KNT (WT*) that has two mutations, Asp80Tyr and Thr130Lys (*9*, *10*). After three successive rounds of screening and selection at increasing temperatures, a mutant named KT3-11 was obtained. To further increase the stability of KT3-11, nine potentially stabilizing mutations, which were found in other mutants obtained after three rounds of directed evolution, were added to KT3-11. The resultant mutant, HTK, has 19 mutations (Figure 1), by which the stability is increased by 20 °C, but the enzyme activity is almost unaltered. The effects of some mutations on the stability of KNT might be explained by the introduction of proline into a β-turn or loop structure (*11*) (mutations at positions 94, 112, 199, and 203) or electrostatic stabilization of the α-helix dipole (*12*) (introduction of arginine at position 91). For other mutations, however, it remains unclear how they stabilize KNT.

In the present study, the contribution of each mutation of HTK to the increased stability and effects of the mutations on the protein structure have been examined, and the mechanism of how these mutations stabilize KNT has been proposed.

† This work was supported in part by the National Project on Protein Structural and Functional Analyses promoted by the Ministry of Education, Science, Sports, Culture, and Technology of Japan.

* To whom correspondence should be addressed. Phone: +81-72-683-1221 (ext. 2644). Fax: +81-72-684-6516. E-mail: med001@art.osaka-med.ac.jp.

‡ Osaka Medical College.

§ RIKEN Genomic Sciences Center.

|| Osaka University.

⊥ RIKEN Harima Institute at SPring-8.

[1] Abbreviations: DTNB, 5,5′-dithiobis(2-nitrobenzoic acid); KNT, kanamycin nucleotidyltransferase; HTK, a highly thermostable KNT with 19 mutations; MD, molecular dynamics; rms, root mean square; rmsd, root-mean-square deviation; WT*, a mutant of the *Staphylococcus aureus* KNT that has two substitutions, Asp80Tyr and Thr130Lys.

10.1021/bi034776z CCC: $25.00
Published on Web 11/20/2003

A

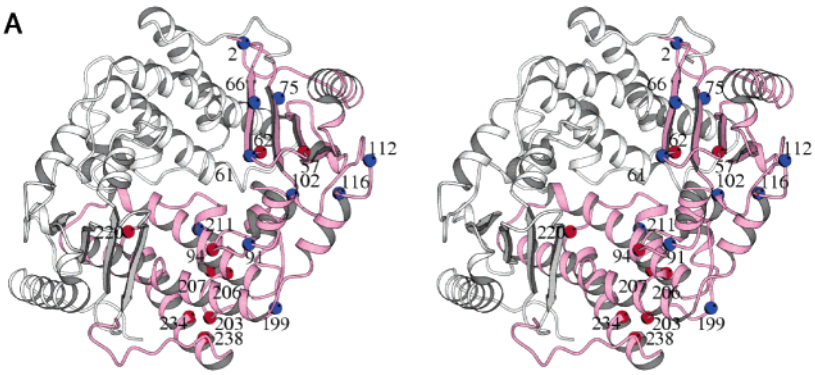

B

Residue No.	2	57	61	62	66	75	91	94	102	112	116	199	203	206	207	211	220	234	238
WT*	N	M	E	A	H	V	Q	S	Q	S	L	S	S	D	H	F	S	I	T
KT3-11	K		G		Y	A	R		R	P	F	P				L			
HTK	K	L	G	V	Y	A	R	P	R	P	F	P	P	V	Q	L	P	V	A

FIGURE 1: Stereo representation of the structure of KNT (A) and amino acid substitutions of KT3-11 and HTK (B) (*7*). The 10 residues mutated in KT3-11 are shown in blue, and the additional 9 residues mutated to construct HTK are in red. In this (A) and other figures of the KNT structures (produced using MOLSCRIPT (*22*), the positions of the residues are shown only for subunit A (pink).

MATERIALS AND METHODS

Site-Directed Mutagenesis and Plasmid Constructions. To construct the KNTs, except for the two KNTs described below, shown in Tables 1 and 2 and Figure 6, the site-directed mutagenesis was performed on an appropriate KNT gene, such as KT3-11 or WT*, subcloned into pUT7 (*7*) using the Sculptor *in vitro* mutagenesis system (Amersham Pharmacia Biotech) or the QuikChange site-directed mutagenesis kit (Stratagene). Lys2 of KT3-11 was mutated back to Asn by PCR with a 5′ primer, 5′-GACTGTACGcatatgAATGGACCAATAATAATGAC-3′ (*Nde*I site in lowercase letters), and a 3′ primer, K3X, 5′-GACTGTACGctcgagCGTAACCAACATGATTAACA-3′ (*Xho*I site in lowercase letters). The amplified KT3-11 (K2N) gene was then subcloned into the *Nde*I and *Xho*I sites of pUT7. Leu211 of KT3-11 was mutated back to Phe as follows: First, the coding region of the WT* gene was subcloned into pUC18, the resultant plasmid, pUC18-WT*KNT, was digested with *Eco*RI and *Bgl*II, and the larger fragment, which contains Phe211, was gel-purified. Next, the smaller *Eco*RI−*Bgl*II fragment of KT3-11 was ligated with the pUC18-WT*KNT fragment. The resultant KT3-11 (L211F) gene was then subcloned into pUT7. The nucleotide sequences of the entire coding regions of all the mutants constructed as above were verified.

To incorporate a 6His-tag sequence at the N-terminus of KNT, the coding region was amplified by PCR and subcloned into the *Nde*I and *Xho*I sites of pUT7. The PCR primers were a pair of one of the following 5′ primers and K3X:5′-GACTGTACGcatatgCAGCAGCAGCAGCAGCAGAATGGACCAATAATAATGAC-3′ (for WT* and cysteine mutants of WT*); 5′-GACTGTACGcatatgCAGCAGCAGCAGCAGCAGAAAGGACCAATAATAATGAC-3′ (for HTK and cysteine mutants of HTK) (*Nde*I site in lowercase letters).

Expression and Purification of KNTs. WT* and HTK were expressed and purified as described previously (*7*). The expression and purification of the KNTs with the His-tag were done as follows: *Escherichia coli* BL21(DE3) pLysS cells carrying the expression plasmid were grown in a medium containing 1.0% polypepton, 0.5% yeast extract, and 1.0% NaCl (adjusted to pH 7.0 with NaOH) supplemented with 100 μg/mL ampicillin and 1 mM isopropyl 1-thio-β-D-galactoside for 16 h at 37 °C. The cells were harvested, resuspended in 20 mM Tris−HCl buffer, pH 7.9, containing 500 mM NaCl and 5 mM imidazole, and disrupted by sonication. The supernatant of the lysate after centrifugation was applied on a His·Bind resin column (Novagen) equilibrated with the above buffer, washed, and then eluted with the buffer containing 100 mM imidazole according to the manufacturer's instructions. The fractions were checked by SDS−PAGE. All the following procedures were done at 4 °C. The fractions containing KNT were pooled and dialyzed against 10 mM potassium phosphate buffer, pH 7.0. The dialyzed solution was applied on an Econo-Pac CHT-II cartridge (hydroxyapatite) column (Bio-Rad Laboratories) equilibrated with the dialysis buffer, which was connected to an FPLC system, and then eluted with a linear gradient of 10−100 mM potassium phosphate over 30 min at a flow rate of 1.0 mL/min.

KNT Assay. The reactions were done at 25 °C in 50 mM NaMES buffer, pH 6.0, containing 50 mM $MgCl_2$, 2 mM kanamycin, and 5 mM ATP (containing 2.1 mCi/mol [8-^{14}C]-ATP). The product was separated on thin-layer chromatography plates and quantified using a Fujifilm phosphorimager, BAS-2000, as described previously (*7*).

Heat Inactivation Assay. Crude *E. coli* lysates (50 μL) containing KNT mutants were incubated at indicated temperatures for 10 min in a heating block filled with water, chilled quickly on ice, and then centrifuged at 15000*g* for 15 min at 4 °C. The KNT activity of each supernatant was measured at 25 °C and compared to that of the supernatant of the nonheated lysate containing the same mutant.

Molecular Dynamics (MD) Simulations. The MD simulations of WT* and HTK were carried out for 1 ns at 345 K (72 °C). The X-ray crystallographic coordinate of KNT at 2.8 Å resolution (*13*) (PDB entry 1KNY) was used as the starting model structure. This coordinate includes a dimer KNT, two ATP analogues (adenosine 5′-α,β-methylene-

triphosphate), and two kanamycin molecules in a crystallographic asymmetric unit. This *S. aureus* KNT has a single amino acid substitution (Asp80Tyr).

The initial coordinates of two KNTs for the MD simulation were constructed using the molecular modeling programs Xfit (*14*) and X-PLOR (*15*). WT* has another amino acid substitution (Thr130Lys). This amino acid substitution was introduced into each subunit. The ATP analogue and kanamycin were removed from the starting coordinate, while the crystal waters were retained. All the hydrogen atoms were generated with the HBUILD routine of X-PLOR. Then, 500 steps of Powell energy minimization were done in a vacuum using X-PLOR to remove any strains in the modified structure. HTK has 19 additional amino acid substitutions to WT*. The same procedure was done to construct the HTK initial coordinate.

A solvation sphere with a 45.6 Å radius was employed to solvate the entire dimer structure by a 7 Å thick water shell as follows: The solvation sphere was constructed by covering the spherical domain with three-dimensional cubic grids and randomly placing TIP3P water (*16*) in each cube. The grid spacing of 3.1 Å was chosen, resulting in a density of 1.0 g/cm^3. To obtain the proper geometry for each water molecule, 300 steps of Powell energy minimization were done. The system was equilibrated at 345 K for 5 ps using X-PLOR. Each KNT was centered within this preconstructed sphere of water. All water molecules having one of their atoms closer than 2.8 Å to the atoms of KNT or to the crystal water molecules were removed. To achieve electroneutrality for the system, sodium ions were added by replacing water molecules of the highest electrostatic energies on the oxygen atom, located more than 9 Å from each other, and 5 Å from the KNT atoms: 18 sodium ions for WT* and 12 sodium ions for HTK. Finally, 500 steps of Powell energy minimization were done using X-PLOR. The total number of atoms in the two resulting systems was 37908 for WT* and 37968 for HTK.

All simulations were carried out using the molecular dynamics program NAMD 2.5b1 (*17*, *18*) with version 22 of the CHARMM force field parameter set (*19*) on IBM RS/6000 SP and pSeries 690-Regatta. In all the simulations, a time step of 1 fs was used to calculate the equations of motion, and a temperature rescaling was done every 100 time steps (every 100 fs). The dielectric constant, $\epsilon = 1$, was assumed, and no boundary condition was used. To reduce the quantity of this MD simulation, the following two procedures were done: (i) For the nonbonded interactions, the force shift option was used to cause the interaction energies and forces to vanish smoothly at a distance of 12 Å. (ii) All bond lengths involving hydrogens were kept fixed using the SHAKE algorithm (*20*). An initial velocity distribution corresponding to 345 K was assigned to the system. The coordinates were saved every 0.25 ps for later analysis.

Covariances ($S_{i,j}$) of the spatial displacements of the two atoms, *i* and *j*, over the dynamics trajectory were calculated using X-PLOR as follows:

$$S_{i,j} = \frac{\langle x[i]\, x[j]\rangle}{(\langle x[i]^2 - x[j]^2\rangle)^{1/2}}$$

where $x[i]$ or $x[j]$ is the coordinate displacement relative to the average position of atom *i* or *j*, respectively, at a time point and the angular brackets express the average value.

Table 1: Effect of Each Substitition of KT3-11 on Thermostability

KT3-11 mutants[a]	residual activity (%)[b] 65 °C, 10 min	67 °C, 10 min	KT3-11 mutants[a]	residual activity (%)[b] 65 °C, 10 min	67 °C, 10 min
no mutation (KT3-11)	52	10	R102Q	10	0
K2N	59	30	P112S	5	0
G61E	20	2	F116L	1	0
Y66H	46	16	P199S	34	9
A75V	54	22	L211F	26	5
R91Q	8	0			

[a] Each of the 10 mutations of KT3-11 was mutated back to the WT* sequence. [b] KNT denatures irreversibly. Activity measurements were done at 25 °C after heat treatments of the *E. coli* lysate containing each mutant.

Chemical Modification of Cysteine Residues. Chemical modification of the cysteine residues was done in 50 mM Tris−HCl buffer, pH 8.0, at 37 °C in the presence of 0.2 mM 5,5′-dithiobis(2-nitrobenzoic acid) (DTNB) using purified proteins. Protein concentrations were 5.3 μM. The reactions were spectrophotometrically monitored at 412 nm using a Hitachi spectrophotometer, U-3300. The number of modified cysteines was calculated using a molar extinction coefficient of the resultant product, nitrothiobenzoate, $\epsilon_{412} = 14100\ \mathrm{M^{-1}\cdot cm^{-1}}$ (*21*).

RESULTS

Contributions of Individual Mutations to Thermostability. During three rounds of the directed evolution experiments, no selected clones were sequenced, nor were any particular mutations added to or removed from the clones. Thus, after obtaining KT3-11, which was the most stable among 20 clones (only 10 clones were examined in ref *7*), the effects of the 10 mutations of KT3-11 on the stability were examined. All the substitutions of KT3-11 were mutated back to the WT* sequence one at a time, and each "single revertant" of KT3-11 was expressed in *E. coli*. The stablity of each mutant in the crude lysate was compared to that of KT3-11 (Table 1). Although the assays were not done with purified proteins and thus not reliable enough to detect small changes, the following mutations were found to significantly increase the stability of KNT: Glu61Gly, Gln91Arg, Gln102Arg, Ser112Pro, Leu116Phe, and Phe211Leu. One mutation, Asn2Lys, appears to slightly decrease the stability of KT3-11. The effects of the other mutations were not large enough to be detected by this method.

Next, the effects of the nine mutations that were added to KT3-11 to create HTK were examined. Each mutant of KT3-11 was expressed in *E. coli*, and its stability in the crude lysate was compared to that of KT3-11 (Table 2). Four mutations, Met57Leu, Ala62Val, Ser94Pro, and Thr238Ala, significantly increase the stability of KT3-11. The effects of these mutations are approximately additive. The other five mutations show little or no effect on the stability of KT3-11 when added individually, but these mutations dramatically increase the stability when all five mutations are simultaneously added.

MD Simulation at 72 °C. (1) Time Dependency of the Root-Mean-Square Deviation (rmsd). The time course of

Table 2: Effects of Additional Mutations on the Thermostability of KT3−11

KT3-11 mutants[a]	residual activity (%) after 10 min of heat treatment[b] 68 °C	70 °C	75 °C
no mutation (KT3-11)	21	2	0
M57L	47	27	−
A62V	60	21	0
S94P	27	7	−
S203P	19	6	−
D206V + H207Q	20	7	−
S220P	18	3	−
I234V	23	2	−
T238A	35	9	−
A62V + S94P	−	32	0
M57L + A62V + S94P + V238A	−	40	7
M57L + A62V + S94P + S203P + D206V + H207Q + S220P + I234V + T238A	−	84	49

[a] The mutations indicated were added to KT3-11. [b] A dash indicates not examined.

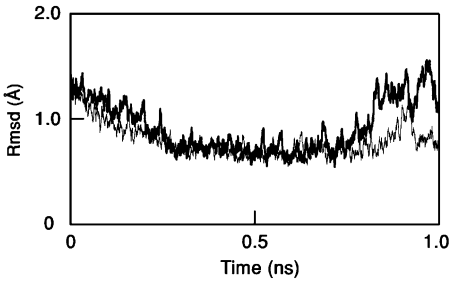

FIGURE 2: Time course of rmsd's of Cα atoms from the corresponding atoms of the average structures during the MD simulations. The rmsd's of WT* (thin line) and HTK (thick line) from the average structures were calculated every 0.25 ps. The average structures were calculated using the coordinates over the 0.25−0.81 ns period.

rmsd from the initial structure was examined (Figure S1 in the Supporting Information): The rmsd of WT* rises during the first 0.25 ns of the simulation time and then fluctuates around a stable value. Although the initial fluctuation of the rmsd of HTK is similar to that of WT*, the rmsd of HTK rises significantly after 0.81 ns. The average structure of each protein was calculated using the coordinates over a 0.56 ns period (0.25−0.81 ns). The time course of rmsd from the average structure (Figure 2) showed that HTK underwent a transition to another metastable structure (Figure S2 in the Supporting Information) at 0.81 ns. Such conformational transition is not evident in WT*, although the rmsd increases transiently around 0.91 ns (Figure 2). The coordinates during the 0.81−1 ns period gave essentially the same results in the subsequent analyses as those during the middle 0.56 ns period (data not shown). Thus, the results obtained for the 0.56 ns period are shown in the present paper.

(2) Average Structures of WT and HTK.* The average structure of HTK was compared to that of WT* (data not shown). All of the secondary structures observed in WT* are maintained in HTK. The rmsd between 506 Cα atoms of the dimers of WT* and HTK is 1.07 Å, and there is no drastic difference between the overall structures.

(3) Fluctuations of WT and HTK Structures.* To analyze the features of the dynamic behavior, the root-mean-square (rms) positional fluctuations of the Cα atoms from the positions of the corresponding atoms in the average structure were calculated for WT* and HTK (Figure 3). Structural fluctuations of HTK are similar to those of WT* for both subunits.

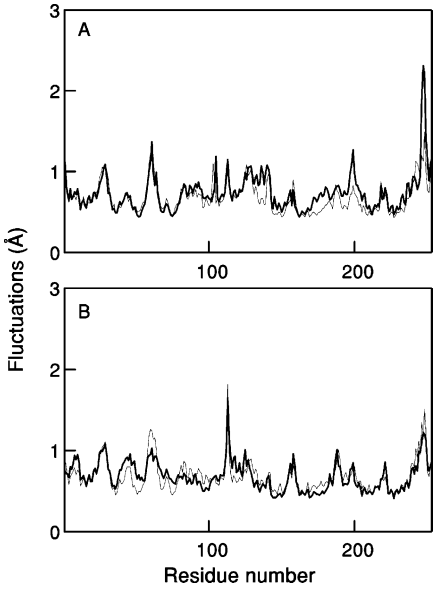

FIGURE 3: Rms positional fluctuations of each Cα atom of WT* (thin lines) and HTK (thick lines) during the MD simulations. The rms positional fluctuations were calculated over each trajectrory after rigid body alignment against each subunit of the average structures. The results for the two subunits A and B are shown in (A) and (B), respectively.

(4) Intradomain and Interdomain Fluctuations. For the analysis of the intradomain and interdomain fluctuations, rigid body alignments were performed for the N-terminal domain (residues 1−130) or the C-terminal domain (residues 131−253) of the KNT structures in each trajectory against the corresponding domain of the average structure, and then the fluctuations of the Cα atoms were calculated and plotted (Figure 4). The calculations were done only for subunit A. For example, the fluctuations in the N-terminal and the C-terminal regions in Figure 4A show those of the N-terminal domain relative to the C-terminal domain (interdomain) and those within the C-terminal domain (intradomain), respectively. The intradomain fluctuations are small and almost the same for the two KNTs. The interdomain fluctuations in Figure 4A clearly show four triangular signals, which are more evident in HTK. The peaks of the triangles are at positions 29, 61, 83, and 113. The fluctuations of the C-terminal domain relative to the N-terminal domain show a single large triangle in HTK at position 156 (Figure 4B). A large peak is observed in the C-terminal region in both the interdomain and intradomain fluctuations (Figure 4). This is because the C-terminal tail of one subunit is attached to the N-terminal domain of the other subunit.

(5) Motional Coupling between Residues. The motional coupling between all pairs of KNT residues was analyzed using a covariance plot constructed from the Cα atom coordinates over the trajectory. In HTK (upper right half of Figure 5), two clusters of residues corresponding to the N- and C-terminal domains are clearly seen in each subunit although the clustering is less evident for the C-terminal domain of subunit A. This means that residues in each domain of HTK move *en bloc* in the same direction at any time point (purple triangular areas near the diagonal). It is

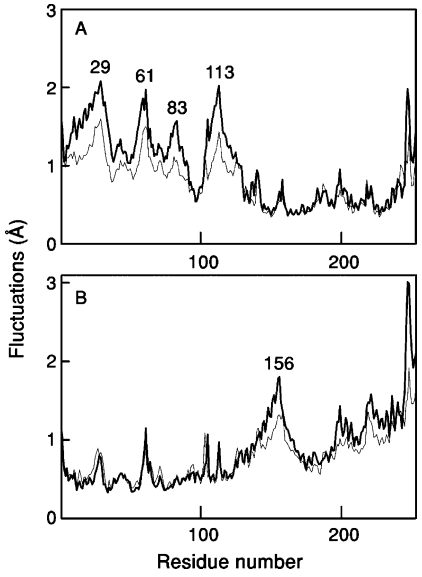

FIGURE 4: Intradomain and interdomain fluctuations of WT* (thin lines) and HTK (thick lines) during the MD simulations. The rms positional fluctuations were calculated over each trajectory after rigid body alignment against the coordinations of the C-terminal domain (residues 131−253) (A) or the N-terminal domain (residues 1−130) (B) of the average structures.

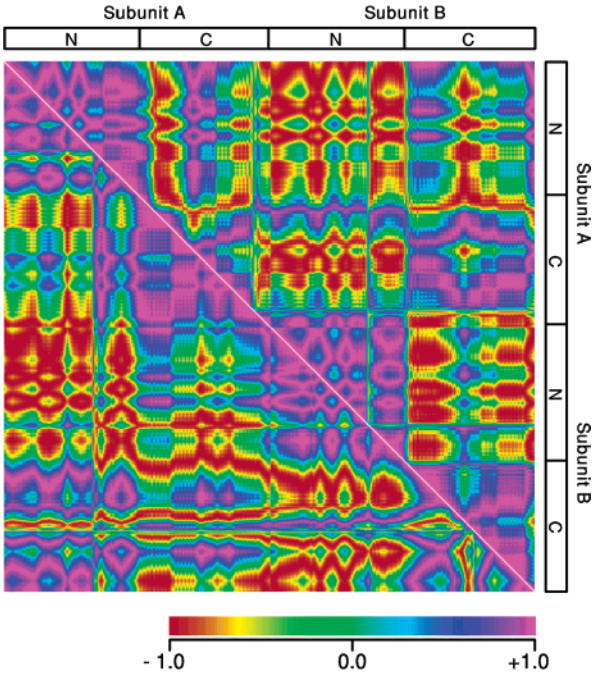

FIGURE 5: Covariance plots of WT* (lower left) and HTK (upper right) residues. Covariance +1 indicates that the motions of the two residues are completely coupled. Covariance −1 indicates that the motions are coupled, but inversely. Covariance 0 indicates that the motions are not coupled at all. The color scale is shown at the bottom.

also shown that the N-terminal domains of the two subunits of HTK move roughly in the opposite direction (red square corresponding to the N(A)−N(B) section). On the other hand, such coordination of movement cannot be observed for WT* (lower left half of Figure 5). Although some pattern is seen in the covariance plot of WT*, the plot of the distance matrix of the WT* residues shows a basically similar pattern (data not shown). Thus, the pattern in the covariance plot of WT*

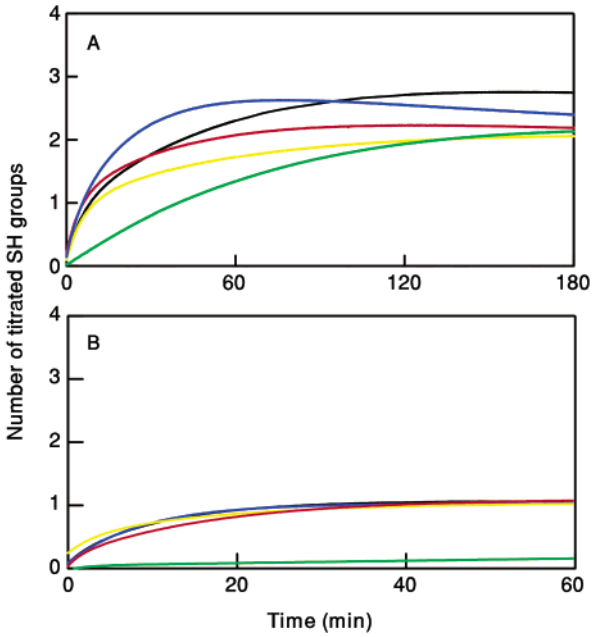

FIGURE 6: Time courses of SH group titrations of WT* (A), HTK (B), and their cysteine mutants. WT* and HTK are shown by black lines. The Cys55Ala, Cys136Ala, Cys184Ala, and Cys209Ala mutants are shown by red, blue, green, and yellow lines, respectively. The reactions were done at 37 °C in the presence of 0.2 mM DTNB at a protein concentration of 5.3 μM. The titration curves of HTK and its mutants showed no further changes after 60 min (B). All the results in this figure were obtained with His-tagged proteins. It was confirmed that the titration curves of WT* and HTK with the His-tag are indistinguishable from those of the corresponding proteins without the His-tag (data not shown).

would simply reflect that spatially close residues or those in a given secondary structure tend to move together.

Chemical Modification of Cysteine Residues. Time courses of the titrations with an SH reagent, DTNB, are shown in Figure 6. Three SH groups are modified in WT*, while only one group is in HTK (black lines). Both WT* and HTK have four cysteine residues per subunit. To identify which cysteine residues are modified, each cysteine was mutated to alanine, and an SH group titration was done. Among the mutants of WT*, only the Cys136Ala mutant has its three cysteines modified (blue line in Figure 6A), indicating Cys136 is the residue that is not modified in WT*. On the other hand, the only residue modified in HTK was found to be Cys184 (green line in Figure 6B). The titration curve of the Cys184Ala mutant of WT* (green line in Figure 6A) has lost the initial fast phase observed in those of WT* and other WT* mutants. These findings indicate that Cys184 is modified most readily among the four cysteines.

DISCUSSION

As summarized in Figure 7, the mutations were divided into three groups on the basis of the extent of their effects on the stability (Tables 1 and 2). All mutations with large effects (red in Figure 7) are located in the N-terminal domain. Although two C-terminal domains extensively interact with each other to form the subunit interface, the N-terminal domains mainly protrude into the solvent and, therefore, might be a structural weak point. This idea would explain why mutations with large effects were accumulated in this domain during the course of the directed evolution.

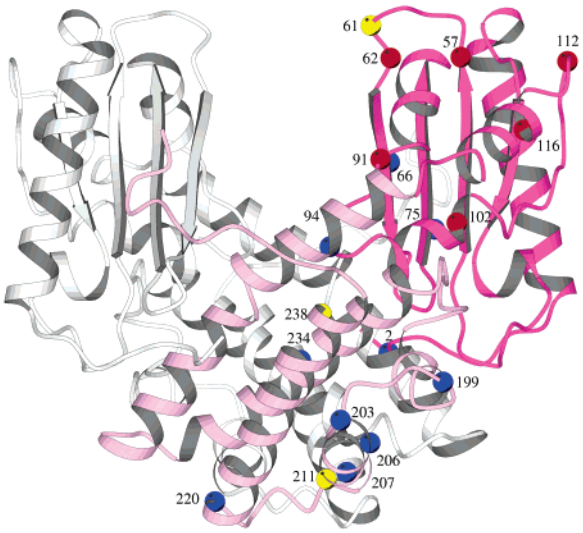

FIGURE 7: Classification of mutations. The 19 mutations were divided into three groups on the basis of the data in Tables 1 and 2: Those with large effects on the thermostability are shown in red, those with moderate effects are in yellow, and those with small or undetectable effects are in blue. This figure is viewed perpendicular to the 2-fold axis of the dimer structure. The N-terminal domain is drawn in purple, and the C-terminal domain is in pink.

As shown in Table 2, the effects of some mutations (Ser203Pro, Asp206Val, His207Gln, Ser220Pro, and Ile234Val) seem to be negligible when added individually. These mutations, however, dramatically increase the stability of KNT when added simultaneously, implying that these mutations work cooperatively. The analysis of the evolved *p*-nitrobenzyl esterase indicates cooperative mutations (*6*). The Tyr66His and Ala75Val mutations show no effects in Table 1 but were found in 18 and 20, respectively, out of 20 independent clones obtained after three rounds of directed evolution (data not shown). Such highly conserved mutations should be important for the stabilization of KNT, and thus, these two mutations might also work cooperatively with each other or with some other mutation(s). The existence of cooperativity among the mutations implies that, to elucidate the effect of each mutation on the structure of KNT, we need to construct and analyze mutants with all the combinations of the 19 mutations, which is practically impossible. Therefore, we examined how the 19 mutations, as a whole, affect the structure of KNT.

We first tried crystallization of HTK under various conditions but obtained very small crystals of poor quality. Therefore, molecular dynamics simulations were performed to analyze the structure at 72 °C. At this temperature, WT* is completely denatured in seconds, while HTK remains native for at least 10 min in the thermal denaturation experiments (*7*). The averaged overall structure, or the static structure, of HTK is almost the same as that of WT* (data not shown). On the other hand, dynamic structures were found to be significantly different between these two KNTs. Despite our initial expectation that HTK would be structurally more rigid than WT*, the structural fluctuations of HTK are similar to those of WT* in Figure 3. The fluctuations were then divided into intradomain and interdomain fluctuations (Figure 4). In Figure 4A, four triangle-shaped signals are observed in the N-terminal region. The peaks of the triangles are located at the tips of the N-terminal domain (Figure 8), and the bottoms correspond to the domain interface. However, these signals have almost disappeared in Figure 4B. The peak of a large single triangle in Figure 4B is also located at a bottom tip of the C-terminal domain (Figure 8) and has reduced its size in Figure 4A. These findings indicate that the N-terminal domain is fluctuating in a hingelike motion relative to the C-terminal domain, the bending point of which is at the domain interface, while the overall configuration of each domain is maintained. Such hingelike motion was observed for HTK in the conformational transition during the time course of the simulation (Figure S2). The substitution of proline for Ser112, which is next to the position of the peak of one triangle in Figure 4A, may affect the flexibility of the loop structure and help the N-terminal domain to move *en bloc*. To further analyze the dynamic characteristics, motional coupling of the residues was compared between WT* and HTK in the covariance plots (Figure 5). The covariance plot of HTK shows that the motions of the residues in each domain are coupled, whereas that of WT* shows no such coordinated motions. Such

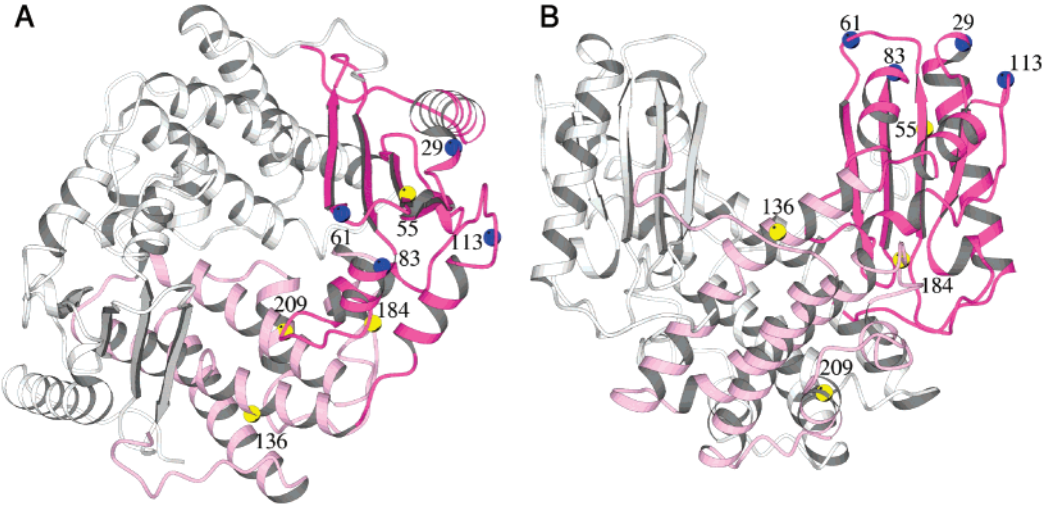

FIGURE 8: Locations of the residues corresponding to the positions of the peaks in Figure 4A (blue) and cysteine residues (yellow). The structures viewed along the 2-fold axis of the dimer structure and perpendicular to the 2-fold axis are drawn in (A) and (B), respectively. The N-terminal domain is drawn in purple, and the C-terminal domain is in pink.

dynamic features of the domain structures would be equivalent to the notion that each domain of HTK is actually more rigid than that of WT* despite similar fluctuations in Figure 3. For HTK, the increased thermal energy would result in larger interdomain motions as shown in Figure 4 because the increased rigidity reduces the intradomain fluctuations. On the other hand, the domain structures of WT* fluctuate randomly at high temperatures, causing thermal denaturation.

To experimentally confirm the above idea, resistances to protease digestion and chemical modification of the cysteine residues were examined. Although definitive results were not obtained by trypsin, lysyl endopeptidase, or V8-protease digestion (data not shown), modification of the cysteine residues clearly supports HTK being structurally more rigid than WT*. Three of four cysteines are modified by DTNB in WT*, while only one cysteine, Cys184, is modified in HTK (Figure 6). Cys55 and Cys209, which are modified in WT* but not in HTK, are located in the N-terminal and C-terminal domains, respectively (Figure 8). This supports both domains of HTK being more rigid than those of WT*. The cysteine residue that is protected from the SH reagent in WT* is Cys136. The number of titrated SH groups of the Cys136Ala mutant of WT* appears to decrease after rapidly reaching its maximum at around 60 min (Figure 6A). This configuration of the titration curve might be caused by some structural perturbation by the mutation of such a strictly protected cysteine residue. Cys184 is located around the domain interface (Figure 8) or the putative bending point of the interdomain motion. This might explain why Cys184 is accessible to the SH reagent even in HTK.

Conclusions. The present results show that the 19 mutations selected by directed evolution stabilize KNT by increasing the rigidity of the domain structures. Each subunit of KNT comprises two relatively distinct domains. It is thus reasonable that the rigidity of each domain, not the whole subunit, is increased. As a result, the hingelike interdomain motion becomes more apparent in HTK. The domains would not be totally independent folding units, however, because single-phase transitions were observed in the thermal denaturation curves of WT*, KT3-11, and HTK (*7*). It would be interesting to analyze how motions on the nanosecond time scale reported here affect the millisecond denaturation process. It is not known at present how the 19 mutations increase the rigidity, but the elucidation of the roles of the mutated residues would deepen our understanding of the structure formation of proteins.

ACKNOWLEDGMENT

We thank Hiroshi Umeda for help in using IBM RS/6000 SP and pSeries 690-Regatta.

SUPPORTING INFORMATION AVAILABLE

Two figures concerning the MD simulations, Figure S1 showing the time courses of the rmsd's of the Cα atoms from the initial structures and Figure S2 showing two time-averaged structures of HTK. This material is available free of charge via the Internet at http://pubs.acs.org.

REFERENCES

1. Arnold, F. H. (2001) *Nature 409*, 253−257.
2. Yano, T., Oue, S., and Kagamiyama, H. (1998) *Proc. Natl. Acad. Sci. U.S.A. 95*, 5511−5515.
3. Oue, S., Okamoto, A., Yano, T., and Kagamiyama, H. (1999) *J. Biol. Chem. 274*, 2344−2349.
4. Shimotohno, A., Oue, S., Yano, T., Kuramitsu, S., and Kagamiyama, H. (2001) *J. Biochem. 129*, 943−948.
5. Moore, J. C., Jin, H.-M., Kuchner, O., and Arnold, F. H. (1997) *J. Mol. Biol. 272*, 336−347.
6. Spiller, B., Gershenson, A., Arnold, F. H., and Stevens, R. C. (1999) *Proc. Natl. Acad. Sci. U.S.A. 96*, 12305−12310.
7. Hoseki, J., Yano, T., Koyama, Y., Kuramitsu, S., and Kagamiyama, H. (1999) *J. Biochem. 126*, 951−956.
8. Yokoyama, S., Hirota, H., Kigawa, T., Yabuki, T., Shirouzu, M., Terada, T., Ito, Y., Matsuo, Y., Kuroda, Y., Nishimura, Y., et al. (2000) *Nat. Struct. Biol. 7*, 943−945.
9. Matsumura, M., and Aiba, S. (1985) *J. Biol. Chem. 260*, 15298−15303.
10. Liao, H., McKenzie, T., and Hageman, R. (1986) *Proc. Natl. Acad. Sci. U.S.A. 83*, 576−580.
11. Matthews, B. W., Nicholson, H., and Becktel, W. J. (1987) *Proc. Natl. Acad. Sci. U.S.A. 84*, 6663−6667.
12. Sali, D., Bycroft, M., and Fersht, A. R. (1988) *Nature 335*, 740−743.
13. Pederson, L. C., Benning, M. M., and Holden, H. M. (1995) *Biochemistry 34*, 13305−13311.
14. McRee, D. (1999) *J. Struct. Biol. 125*, 156−165.
15. Brünger, A. T. (1992) *X-PLOR, Version 3.1. A system for X-ray crystallography and NMR*, Yale University Press, New Haven.
16. Jorgensen, W., Chandrasekhar, J., Madura, J., Impey, R., and Klein, M. (1983) *J. Chem. Phys. 79*, 926−935.
17. Nelson, M., Humphrey, W., Gursoy, A., Dalke, A., Kalë, L., Skeel, R., and Schulten, K. (1996) *J. Supercomput. Appl. 10*, 251−268.
18. Kalë, L., Skeel, R., Bhandarkar, M., Brunner, R., Gursoy, A., Krawetz, N., Phillips, J., Shinozaki, A., Varadarjan, K., and Schulten, K. (1999) *J. Comput. Phys. 151*, 283−312.
19. MacKerell, A. D., Jr., Wiorkiewicz-Kuczera, J., and Karplus, M. (1995) *J. Am. Chem. Soc. 117*, 11946−11975.
20. Ryckaert, J., Ciccotti, G., and Berendson, H. (1977) *J. Comput. Phys. 23*, 327−341.
21. Riddles, P. W., Blakeley, R. L., and Zerner, B. (1979) *Anal. Biochem. 94*, 75−81.
22. Kraulis, P. J. (1991) *J. Appl. Crystallogr. 24*, 946−950.

BI034776Z